

Rayleigh-Bénard Convection for Nanofluids for More Realistic Boundary Conditions (Rigid-Free and Rigid-Rigid) Using Darcy Model

Jyoti Ahuja

Department of Mathematics
Post Graduate Government College
Chandigarh, India
E-mail: jyotiahuja1985@gmail.com

Urvashi Gupta

Dr. S. S. Bhatnagar University Institute of Chemical Engineering & Technology
Panjab University, Chandigarh, India
Corresponding author: dr_urvashi_gupta@yahoo.com; urvashi@pu.ac.in

(Received December 7, 2017; Accepted August 7, 2018)

Abstract

In this article, Rayleigh-Bénard convection for nanofluids for more realistic boundary conditions (rigid-free and rigid-rigid) under the influence of the magnetic field is investigated. Presence of nanoparticles in base fluid has introduced one additional conservation equation of nanoparticles that incorporates the effect of thermophoretic forces and Brownian motion and the inclusion of magnetic field has introduced Lorentz's force term in the momentum equation along with Maxwell's equations. The solution of the Eigen value problem is found in terms of Rayleigh number by implementing the technique of normal modes and weighted residual Galerkin approximation. It is found that the stationary as well as oscillatory motions come into existence and heat transfer takes place through oscillatory motions. The critical Rayleigh number for alumina water nanofluid has an appreciable increase in its value with the rise in Chandrasekhar number and it increases moderately as we move from rigid-free to both rigid boundaries. The effect of different nanofluid parameters on the onset of thermal convection for two types of boundaries is investigated.

Keywords- Darcy's law, Brownian motion, Magneto-convection, Chandrasekhar number.

1. Introduction

The thermal instability of a fluid layer in a porous medium has emerged as an evident problem considering its widespread usage across various utility applications such as enhanced oil recovery, storage of agricultural products, geothermal reservoirs and the underground pollutant transport. For Newtonian fluids, a comprehensive work on the problem of Rayleigh-Bénard convection has been done (Chandrasekhar, 1981) while considering different aspects of hydrodynamics and hydromagnetics. Nanofluid is a very prominent and significant term which is being highly discussed over a broad spectrum considering its relevance and usage. A nanofluid is basically a fluid that is formed by suspending particles of nano-sized such as ceramics, metals, oxides, nitrides, and semiconductors in base fluids like water, ethylene glycol, oil etc. The usefulness of these suspensions is also revealed in the study (Choi, 1995) which also emphasizes the importance of nanofluids in enhancing the heat transfer mechanism because of exhibiting enormously high thermal conductivity. In continuation, other researchers (Das et al., 2003; Masuda et al., 1993) confirmed the same results through their experimental work. Due to enhanced thermal properties, it is now used in nuclear power plants (Buongiorno and Hu, 2005) and in delivering drugs (Kleinstreuer et al., 2008). Further, convective instability of nanofluids is considered (Kim et al., 2004) and have shown that the onset of convection is hastened due to the

enhanced thermal conductivity of nanoparticles. (Buongiorno, 2006) suggested a model using the mechanics of nanoparticles and included the effects due to Brownian motion and thermophoretic diffusion. Buongiorno's model was utilized to analyze the thermal instability problems by many others (Tzou, 2008; Nield and Kuznetsov, 2009; Nield and Kuznetsov, 2010). In the past, the modified problem of thermal convection (Bhadauria and Agarwal, 2011; Yadav et al., 2011) is considered to include the impact of rotation.

Magneto-convection refers to the thermal convection under the effect of the applied magnetic field. According to the experimental results, (Heris et al., 2012) the nanoparticles concentration and the strong magnetic field increase the thermal efficiency of thermosyphon considerably. The impact of applied magnetic field/Hall currents on a layer of nanofluid has been studied (Gupta et al., 2013; 2014) and they have shown that the critical Rayleigh number along with critical wave number undergoes an appreciable rise with the rise in magnetic field parameter and considerable fall with the rise in Hall parameter. The authors considered the convection problem for the case of free-free boundaries, which are not realistic for the case of geophysical situations. The present formulation of the thermal convection problem introduces the impact of permeability and vertical magnetic field using the Darcy model for a porous medium for two types of boundaries: both-rigid and rigid-free. The Rayleigh number at which the instability sets in for alumina-water nanofluid has been identified under different boundaries. The problem has great application in geophysics due to the high magnetic field of the earth, its porous structure and owing to more realistic boundary conditions.

2. Conservation Equations using Darcy Model

In a homogenous porous medium, a thin layer of nanofluid (heated from below) is considered. Temperature and volume fraction of nanoparticles are T_h and ϕ_1 at the lower boundary ($z = 0$); and at the upper boundary ($z = d$) is T_c and ϕ_0 ($T_h > T_c, \phi_1 > \phi_0$) as in Figure 1. The gravitational force $\mathbf{g} = (0, 0, -g)$ and the magnetic field $\mathbf{H} = (0, 0, H)$ are acting in the opposite directions. In the porous medium Darcy model (Nield and Kuznetsov, 2009) is incorporated to analyze the stability of the system. The Darcy velocity is denoted by ' \mathbf{v}_D ' i.e. $\mathbf{v}_D = \varepsilon \mathbf{q}$ where \mathbf{q} is the velocity of nanofluid and ε denotes the porosity of the medium.

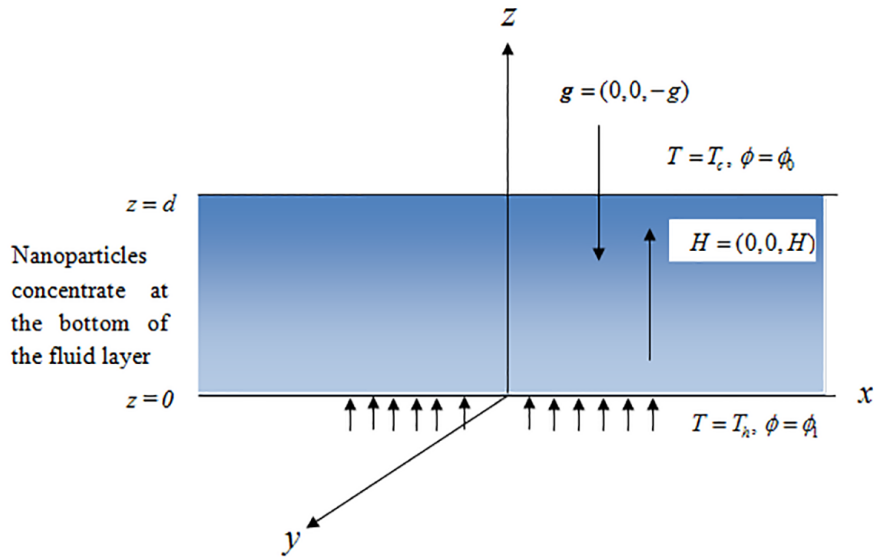


Figure 1. Sketch of the physical system

The hydrodynamic and hydromagnetic equations using the Darcy model and the assumptions as discussed by (Gupta et al., 2013) are

$$\nabla \cdot \mathbf{v}_D = 0, \quad (1)$$

$$\frac{\partial \phi}{\partial t} + \nabla \phi \cdot \frac{\mathbf{v}_D}{\varepsilon} = \nabla \cdot \left[D_T \frac{\nabla T}{T} + \nabla \phi \cdot D_B \right], \quad (2)$$

$$0 = \tilde{\mu} \nabla^2 \mathbf{v}_D - \nabla p + \rho \mathbf{g} - \frac{\mu}{k_1} \mathbf{v}_D + \frac{\mu_e}{4\pi} (\nabla \times \mathbf{h}) \times \mathbf{H}, \quad (3)$$

$$\mathbf{v}_D \cdot \nabla T (\rho c)_f + (\rho c)_m \frac{\partial T}{\partial t} = (k_m \nabla^2 T) + \varepsilon (\rho c)_p \left[D_T \frac{\nabla T \cdot \nabla T}{T} + D_B \nabla T \cdot \nabla \phi \right], \quad (4)$$

The density of nanofluid is denoted by ρ which is given as

$$\rho = \phi \rho_p + (1 - \phi) \rho_f, \cong \phi \rho_p + (1 - \phi) \left\{ \rho_0 (1 - \beta (T - T_0)) \right\}, \quad (5)$$

and Maxwell's equations are

$$\frac{d\mathbf{h}}{dt} = (\mathbf{H} \cdot \nabla) \frac{\mathbf{v}_D}{\varepsilon} + \eta \nabla^2 \mathbf{h}, \quad (6)$$

$$\nabla \cdot \mathbf{h} = 0, \quad (7)$$

where η is the resistivity of the fluid. In order to get the non-dimensional parameter thermal Rayleigh number the above equations are non-dimensionalized by using

$$(x', y', z') = (x, y, z)/d, \quad t' = t\alpha_m/\sigma d^2, \quad h' = (\eta/H\alpha_m)h, \quad (u', v', w') = (u, v, w) d/\alpha_m, \quad p' = pk_1/\mu\alpha_m, \\ \phi' = (\phi - \phi_0)/(\phi_1 - \phi_0), \quad T' = (T - T_c)/(T_h - T_c), \quad \text{where } \alpha_m = k_m/(\rho c)_f, \quad \sigma = (\rho c)_m/(\rho c)_f. \quad (8)$$

After dropping the dashes, Eqs. (1)–(7) are transformed into

$$\nabla \cdot \mathbf{q} = 0, \quad (9)$$

$$0 = -\nabla p - \mathbf{q} - R_m \hat{e}_z - R_{cn} \phi \hat{e}_z + R_a T \hat{e}_z + Q \left[\left(\frac{\partial h_x}{\partial z} - \frac{\partial h_z}{\partial x} \right) \hat{e}_x - \left(\frac{\partial h_z}{\partial y} - \frac{\partial h_y}{\partial z} \right) \hat{e}_y \right], \quad (10)$$

$$\frac{\partial T}{\partial t} + \mathbf{q} \cdot \nabla T = \nabla^2 T + \frac{N_B}{L_h} (\nabla \phi \cdot \nabla T) + \frac{N_A N_B}{L_h} (\nabla T \cdot \nabla T), \quad (11)$$

$$\frac{1}{\sigma} \frac{\partial \phi}{\partial t} + \frac{1}{\varepsilon} \mathbf{q} \cdot \nabla \phi = \frac{1}{L_h} \nabla^2 \phi + \frac{N_A}{L_h} \nabla^2 T, \quad (12)$$

$$\nabla \cdot \mathbf{h} = 0, \quad (13)$$

$$\frac{\varepsilon}{\sigma} \frac{\text{Pr}_2}{\text{Pr}_1} \frac{d\mathbf{h}}{dt} = \left(\frac{\partial u}{\partial z} \hat{e}_x + \frac{\partial v}{\partial z} \hat{e}_y + \frac{\partial w}{\partial z} \hat{e}_z \right) + \varepsilon \nabla^2 \mathbf{h}, \quad (14)$$

where

$\text{Pr}_1 = \mu/\rho\alpha_m$: (the Prandtl number);

$N_A = (D_T(T_h - T_c))/(D_B T_c(\phi_1 - \phi_0))$: the modified diffusivity ratio;

$\text{Pr}_2 = \mu/\rho\eta$: the magnetic Prandtl number;

$L_h = \alpha_m/D_B$: the Lewis number;

$R_a = (\rho g \beta d k_1 (T_h - T_c))/\mu\alpha_m$: the Rayleigh number;

$N_B = [\varepsilon(\rho c)_p/(\rho c)_f](\phi_1 - \phi_0)$: the modified particle-density increment;

$R_m = [\phi_0 \rho_p + \rho(1 - \phi_0)]g d k_1/\mu\alpha_m$: the basic density Rayleigh number;

$R_{cn} = ((\rho_p - \rho)(\phi_1 - \phi_0))/\mu\alpha_m g d k_1$: the concentration Rayleigh number;

and $Q = (\mu_e H^2 k_1/4\pi\eta\mu)$: the Chandrasekhar number. (15)

3. Initial Flow and Perturbation Equations

The initial flow is supposed to be stationary and the temperature, nanoparticle fraction and pressure are assumed to vary in z direction only i.e.

$$\mathbf{q} = 0, \quad T = T_1(z), \quad p = p_1(z), \quad \phi = \phi_1(z). \quad (16)$$

The subscript ‘1’ represents the initial flow. Applying Eq.(16) to Eqs. (10)-(12) and integrating w.r.t. z , we get

$$\phi = -N_A T_1 + (1 + N_A)(1 - z), \quad (17)$$

$$T_1 = \frac{1 - e^{-(1+N_A)N_B(1-z)/L_h}}{1 - e^{-(1+N_A)N_B/L_h}}. \quad (18)$$

As suggested by Buongiorno (2006), L_h is large and N_A is small. By neglecting the second and higher order terms, Eqs. (18) and (17) reduce to

$$T_1 = 1 - z, \quad (19)$$

$$\phi_1 = 1 - z. \quad (20)$$

Let us apply very small perturbations (denoted by bar symbol) on the initial flow

$$\mathbf{q}(u, v, w) = 0 + \bar{\mathbf{q}}, \quad \phi = \phi_1 + \bar{\phi}, \quad p = p_1 + \bar{p}, \quad \mathbf{h}(h_x, h_y, h_z) = \mathbf{H} + \bar{\mathbf{h}}, \quad T = T_1 + \bar{T}, \quad (21)$$

with $T_1 = \phi_1 = 1 - z$. Applying (21) to Eqs. (9)–(14), linearizing and using Eqs. (19) and (20), we get

$$\nabla \cdot \mathbf{q} = 0, \quad (22)$$

$$\nabla^2 w - Q \nabla^2 \frac{\partial h_z}{\partial z} + R_{cn} \nabla_H^2 \phi - R_a \nabla_H^2 T = 0, \quad (23)$$

$$-w + \frac{\partial T}{\partial t} = \nabla^2 T - 2 \frac{N_A N_B}{L_h} \frac{\partial T}{\partial z} - \frac{N_B}{L_h} \left(\frac{\partial \phi}{\partial z} + \frac{\partial T}{\partial z} \right), \quad (24)$$

$$\frac{1}{\sigma} \frac{\partial \phi}{\partial t} - \frac{w}{\varepsilon} = \frac{1}{L_h} \nabla^2 \phi + \frac{N_A}{L_h} \nabla^2 T, \quad (25)$$

$$\zeta - Q \frac{\partial \xi}{\partial z} = 0, \quad (26)$$

$$\frac{\varepsilon}{\sigma} \frac{\text{Pr}_2}{\text{Pr}_1} \frac{\partial \xi}{\partial t} = \frac{\partial \zeta}{\partial z} + \varepsilon \nabla^2 \xi, \quad (27)$$

$$\frac{\varepsilon}{\sigma} \frac{\text{Pr}_2}{\text{Pr}_1} \frac{\partial h_z}{\partial t} - \varepsilon \nabla^2 h_z = \frac{\partial w}{\partial z}, \quad (28)$$

where $\nabla_H^2 = \partial^2 / \partial x^2 + \partial^2 / \partial y^2$ and ∇p is eliminated from Eqs.(23), (27) and (28) by introducing $\zeta = (\partial v / \partial x - \partial u / \partial y)$ and $\xi = (\partial h_y / \partial x - \partial h_x / \partial y)$. The system of differential Eqs. (22)-(28) will be used in further analysis by applying the methodology of superposition of basic modes and one term Galerkin residual approximation.

4. Normal Mode Analysis and Galerkin Type Weighted Residual Method

In the present study, we have used the methodology of superposition of basic modes in which the perturbed quantities are expressed as

$$(w, \xi, T, \zeta, \phi, h_z) = (W(z), X(z), \Theta(z), Z(z), \Phi(z), K(z)) \exp(il_x x + il_y y + nt), \quad (29)$$

where l_x and l_y are the wave numbers in two directions (horizontal and vertical) and n is the growth rate. The linearized equations after the process of elimination are

$$(D^2 - a^2)W - Q(D^2 - a^2)DK - R_{cn}a^2\Phi + R_a a^2\Theta = 0, \quad (30)$$

$$\left\{ \frac{\varepsilon \text{Pr}_2}{\sigma \text{Pr}_1} n - \varepsilon(D^2 - a^2) \right\} K = DW, \quad (31)$$

$$n\Theta - W - \left(D^2 - \frac{N_B}{L_n} D - 2\frac{N_A N_B}{L_n} D - a^2\right)\Theta + \frac{N_B}{L_n} D\Phi = 0, \quad (32)$$

$$\frac{1}{\sigma} n\Phi - \frac{W}{\varepsilon} - \frac{N_A}{L_n} (D^2 - a^2)\Theta - \frac{1}{L_n} (D^2 - a^2)\Phi = 0, \quad (33)$$

where $D \equiv d/dz$ and $a = (l_x^2 + l_y^2)^{1/2}$ is the resultant wave number. Eliminating K from Eqs. (30) and (31), we obtain

$$\left[\left\{ (D^2 - a^2) \right\} \left\{ \frac{\varepsilon \text{Pr}_2}{\sigma \text{Pr}_1} n - \varepsilon(D^2 - a^2) \right\} - QD^2 (D^2 - a^2) \right] W + \left\{ \frac{\varepsilon \text{Pr}_2}{\sigma \text{Pr}_1} n - \varepsilon(D^2 - a^2) \right\} (R_a a^2\Theta - R_{cn} a^2\Phi) = 0. \quad (34)$$

Now in order to solve Eqs. (32)-(34), Galerkin weighted residuals approach is adopted. Choice of the trial functions W_p, Θ_p and Φ_p depends on the relevant boundary conditions and we write

$$W = \sum_{p=1}^N A_p W_p, \quad \Theta = \sum_{p=1}^N B_p \Theta_p, \quad \Phi = \sum_{p=1}^N C_p \Phi_p. \quad (35)$$

For single term approximation, we put $p = 1$. After substituting Eq. (35) in Eqs. (32)-(34) and making use of orthogonality; we obtain a system of three equations in three unknowns A_1, B_1, C_1 . Elimination of these unknowns from the obtained set of equations gives the Eigen value equation.

5. Results and Discussion

5.1 Rigid-Rigid Boundaries

Let us now consider that both the boundaries of the fluid layer are rigid. Therefore, the vanishing of the normal as well as horizontal components of the velocity to the rigid surface (no slip condition) leads to the boundary conditions

$$W = 0, \Phi = 0, \Theta = 0 \text{ and } DW = 0, \text{ at both the boundaries } K = 0, DK = 0, \quad (36)$$

for perfectly conducting boundaries. The suitable trial functions satisfying this boundary condition are

$$\Theta_1 = z(1-z), \quad W_1 = z^2(1-z^2), \quad \Phi_1 = z(1-z). \quad (37)$$

Using the approximation of single term Galerkin residual method and orthogonality, the eigen value equation becomes

$$\begin{aligned} & \left[-\frac{\varepsilon \text{Pr}_2}{\sigma \text{Pr}_1} n \left\{ \frac{2}{105} + \frac{a^2}{630} \right\} - \varepsilon \left\{ \frac{24}{30} + 4 \frac{a^2}{105} + \frac{a^4}{630} \right\} - Q \left\{ \frac{2}{105} + \frac{2a^2}{105} \right\} \right] \left[140 \left(\frac{n}{30} + \frac{a^2}{30} + \frac{1}{3} \right) \right] \\ & \left[\frac{n}{\sigma} \cdot \frac{1}{30} + \left(\frac{a^2}{30} + \frac{1}{3} \right) \frac{1}{L_n} \right] + \left[\frac{\varepsilon \text{Pr}_2}{\sigma \text{Pr}_1} n \cdot \frac{1}{140} + \varepsilon \left\{ \frac{2}{30} + \frac{a^2}{140} \right\} \right] \left[R_a a^2 \left(\frac{n}{\sigma} \cdot \frac{1}{30} \right) + \left(\frac{a^2}{30} + \frac{1}{3} \right) \frac{1}{L_n} \right] \\ & - R_{cn} a^2 \left[\frac{1}{\varepsilon} \left(\frac{n}{30} + \frac{a^2}{30} + \frac{1}{3} \right) - \left(\frac{a^2}{30} + \frac{1}{3} \right) \frac{N_A}{L_n} \right] = 0. \end{aligned} \quad (38)$$

Let us discuss the case of stationary convection by putting $n=0$ in Eq. (38). The expression for Rayleigh number for both rigid boundaries become

$$R_a(\text{stat}) = R_{cn} \left(\frac{L_n}{\varepsilon} - N_A \right) + \frac{140}{a^2 \left(\frac{2}{30} + \frac{a^2}{140} \right)} \left[\left\{ \frac{504 + 24a^2 + a^4}{630} \right\} + \frac{Q}{\varepsilon} \left\{ \frac{168 + 4a^2}{210} \right\} \right] \left(\frac{a^2}{30} + \frac{1}{3} \right). \quad (39)$$

Critical Rayleigh number along with critical wave number is found by the condition $dR_a/da=0$, numerically. In the absence of nanoparticles and magnetic field the value of critical wave number is $a_c=4.791$ and critical Rayleigh number is 72.94. For oscillatory convection we put $n=i\omega \neq 0$ in the Eigen value Eq. (38), and separate the imaginary and real parts to get an expression for $R_u(\text{osc})$. This expression is quite lengthy so we have written it in Appendix B1; nevertheless the same is used to plot the graphs of $R_u(\text{osc})$ for rigid-rigid boundaries.

5.2 Rigid-Free Boundaries

Let us now consider the lower boundary of the fluid to be rigid and the upper as free. The relevant boundary conditions on W are

$$DW = 0, W = 0, \quad \text{at } z = 0 \quad \text{for lower boundary,} \quad (40)$$

$$D^2W = 0, W = 0, \quad \text{at } z = 1 \quad \text{for upper boundary.} \quad (41)$$

Trial function appropriate to these boundaries is

$$W_1 = z^2(1-z)(3-2z). \quad (42)$$

By making use of single term Galerkin method and orthogonality, the Eigen value equation in the present case becomes

$$\begin{aligned} & \frac{420}{13} \left[-\frac{\varepsilon \text{Pr}_2}{\sigma \text{Pr}_1} n \left\{ \frac{12}{35} + a^2 \frac{76}{2520} \right\} - \varepsilon \left\{ \frac{36}{5} + \frac{24a^2}{35} + a^4 \frac{76}{2520} \right\} - Q \left\{ \frac{36}{5} + \frac{12a^2}{35} \right\} \right] \\ & \left(\frac{a^2}{30} + \frac{1}{3} + \frac{n}{30} \right) \left(\frac{1}{L_n} \left(\frac{a^2}{30} + \frac{1}{3} \right) + \frac{n}{30\sigma} \right) + \left\{ \frac{\varepsilon \text{Pr}_2}{\sigma \text{Pr}_1} n \frac{13}{420} + \varepsilon \left\{ \frac{3}{10} + \frac{13}{420} a^2 \right\} \right\} \\ & \left[R_a a^2 \left(\frac{a^2}{30} + \frac{1}{3} + \frac{n}{30\sigma} \right) - R_{cn} a^2 \left\{ \frac{1}{\varepsilon} \left(\frac{a^2}{30} + \frac{1}{3} + \frac{n}{30} \right) - \frac{N_A}{L_n} \left(\frac{a^2}{30} + \frac{1}{3} \right) \right\} \right] = 0. \end{aligned} \quad (43)$$

For stationary convection, the Eigen value Eq. (43) takes the form

$$R_a(\text{stat}) = R_{cn} \left(\frac{L_n}{\varepsilon} - N_A \right) + \frac{420}{a^2(126+13a^2)} \left[\left\{ \frac{4536+432a^2+19a^4}{630} \right\} + \frac{Q}{\varepsilon} \left\{ \frac{252+12a^2}{35} \right\} \right] \left(\frac{a^2}{30} + \frac{1}{3} \right) \frac{420}{13}. \quad (44)$$

Equation (44) attains its minimum value when $a_c=3.97$ and this minimum is 56.97 (taking $Q=0, R_{cn}=0$). For oscillatory modes, the expression for Rayleigh number is found as given in Appendix B2 and the graphs are plotted using the software Mathematica.

Let us now analyze the critical values for alumina-water nanofluid ($L_n=5000, N_A=5$ and fixed $R_{cn}=0.1$) for the two types of boundaries. It has been observed that as the porosity increases there is a fall in the critical wave number and a predominant fall in the critical Rayleigh number for the two type of boundaries (Table 1). This means as the ratio of pore space to total space increases the nanofluid layer system gets strongly destabilized and it hastens the onset of instability. As we move from rigid-free boundaries to both rigid boundaries a_c shows a significant increase along with some increase in R_c i.e. $(R_c)_{\text{both-rigid}} > (R_c)_{\text{rigid-free}}$ which means that the stability of the fluid layer system increases as we move from rigid-free and both-rigid boundaries.

Table 1. Effect of ε for alumina-water nano-fluid on a_c and R_c for $Q=100, R_{cn}=0.1$.

ε	Rigid-Free		Both Rigid	
	a_c	R_c	a_c	R_c
0.2	18.67	9219.44	22.52	9798.28
0.4	15.71	4773.57	18.95	5130.24
0.6	14.20	3268.28	17.13	3540.69
0.8	13.22	2506.61	15.95	2732.95

Table 2. Effect of Q for alumina-water nanofluid on a_c and R_c for $\varepsilon = 0.7$, $R_{cn} = 0.1$.

Q	Rigid-Free		Both Rigid	
	a_c	R_c	a_c	R_c
0	3.97	770.97	4.791	786.94
100	13.67	2834.25	16.49	3080.77
500	20.41	10132.62	24.61	10884.2
1000	24.26	19014.7	29.24	20292.3

In Table 2, a_c and R_c are considered for different values of Q and for $\varepsilon = 0.7$, $R_{cn} = 0.1$. Both a_c and R_c show a tremendous rise with the rise in magnetic field parameter for the two type of boundary conditions. Further a_c and R_c exhibit an increase while moving from rigid-free to both rigid boundaries. This shows that magnetic field bears a strong influence on the nanofluid layer system by way of increasing its stability and delaying the onset of thermal convection.

6. Numerical Results and Discussion

To analyse the behavior of parameters like R_{cn} , Q , ε , L_n , N_A and σ on the onset of convection; computations are carried out using Eqs. (39) and (44) for stationary convection for both-rigid and rigid-free boundaries, respectively. To carry out the computations in respect of oscillatory motions, expressions for $(R_a(osc))_{both\ rigid}$ and $(R_a(osc))_{rigid-free}$ (given in Appendix B1 and Appendix B2 as B.1.1 and B.1.2) are used for rigid-rigid and rigid-free boundaries, respectively. The curves representing the variation of $R_a(stat)$ and $R_a(osc)$ w.r.t the wave number ‘ a ’ for fixed values of other parameters have been sketched. The fixed values of various parameters are taken as $Pr_1 = 1$, $Pr_2 = 0.01$, $R_{cn} = 4$, $L_n = 100$, $Q = 50$, $N_A = 4$, $\varepsilon = 0.7$, $\sigma = 1$. By changing the value of one parameter the effect of that particular parameter can be examined on the convection problem.

Figures 2-11 show the neutral stability curves for non-oscillatory and oscillatory motions in porous medium for bottom heavy configuration of nanoparticles. Figure 2 is a plot of $R_a(stat)$ and Figure 3 is a plot of $R_a(osc)$ versus wave number for $R_{cn} = 4, 7$ and 10 . It is seen that $(R_a)_{both\ rigid} > (R_a)_{rigid-free}$ for both types of convections. If we compare Figures 2 and 3 it is easy to recognize that $R_a(stat) > R_a(osc)$ for fixed ‘ a ’ that means the mode of heat transfer is through oscillatory motions instead of stationary convection. Figure 2 presents a clear picture of the significant increase in $R_a(stat)$ with the rise in R_{cn} whereas there is no significant increase in $R_a(osc)$ (Figure 3). Thus the increase in the concentration of nanoparticles makes the stationary convection much more stable as compared to over stable convection (Figure 3) when particle density decreases upward.

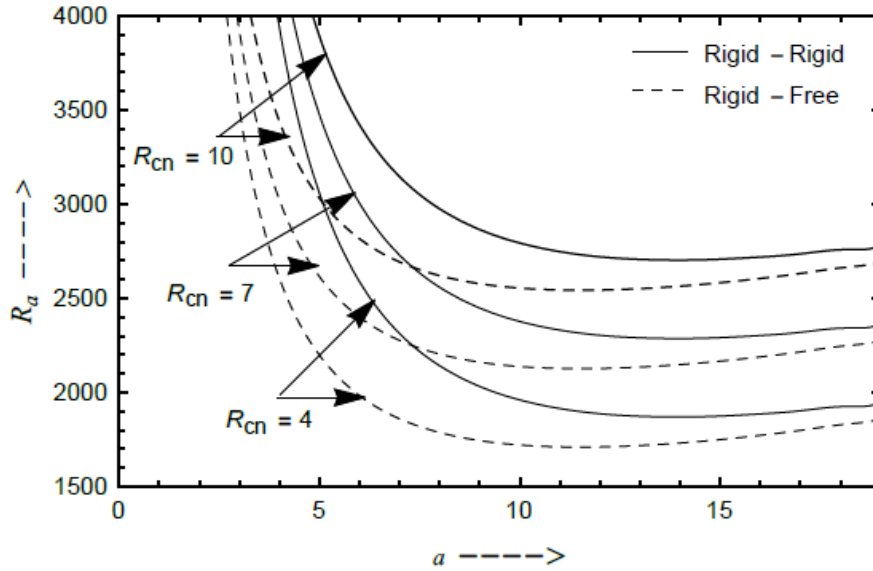


Figure 2. Influence of concentration Rayleigh number on $R_a(stat)$ for $R_{cn}=4, 7$ and 10 for two different boundaries

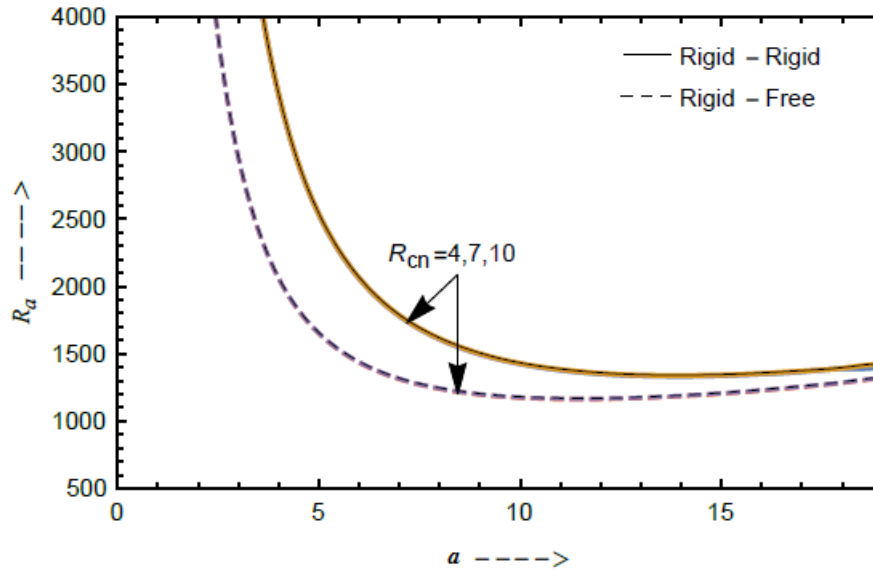


Figure 3. Influence of concentration Rayleigh number on $R_a(osc)$ for $R_{cn}=4, 7$ and 10 for two different boundaries

Figures 4-5 correspond to Rayleigh numbers $R_a(stat)$ and $R_a(osc)$, respectively, for $Q=50, 100$ and 150 . Both these figures show that there is a remarkable enhancement in the

values of $R_a(stat)$ as well as $R_a(osc)$ with the increase in Chandrasekhar number. Thus, the application of magnetic field postpones the onset of convection and this delaying effect grows in magnitude with the rise in the magnetic field. Further, it is interpreted from the figures that the curves showing the effect of the magnetic field for rigid-free boundaries, lies below the curves for both rigid boundaries. The fluid layer confined between both rigid boundaries is more stable as compared to rigid-free boundaries. Figure 4-5 show that $R_a(stat) > R_a(osc)$ for all values of the Chandrasekhar number maintaining the fact that oscillatory motions prevail the system.

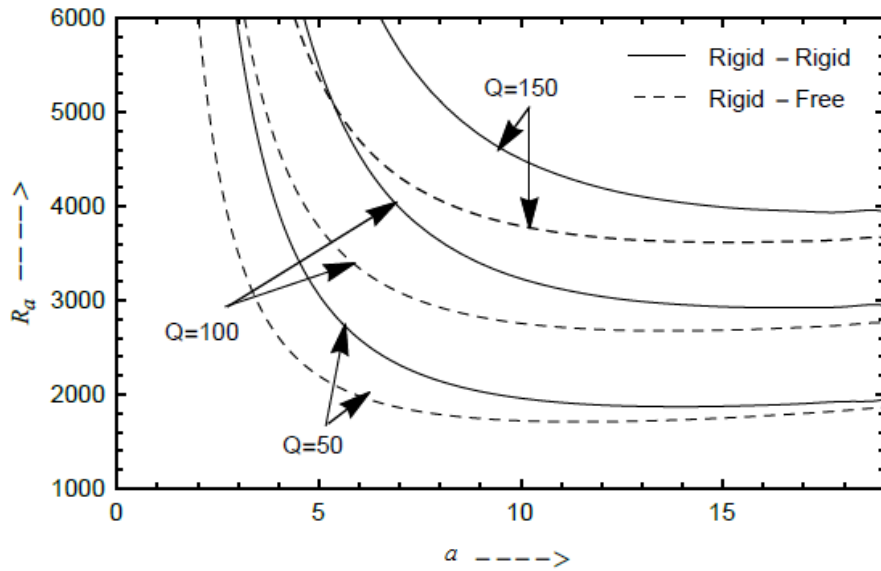


Figure 4. Influence of magnetic field on $R_a(stat)$ for $Q=50, 100$ and 150 for two different boundaries

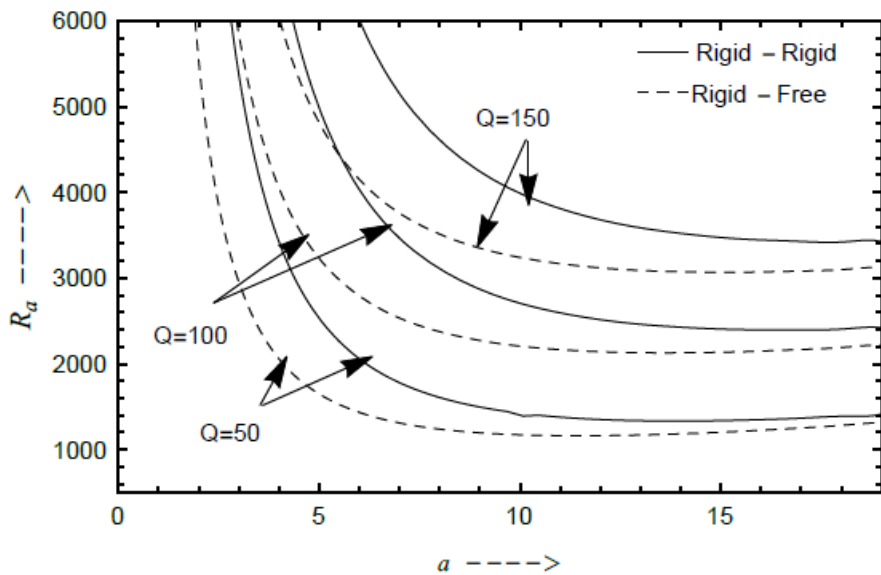


Figure 5. Influence of magnetic field on $R_a(osc)$ for $Q=50, 100$ and 150 for two different boundaries.

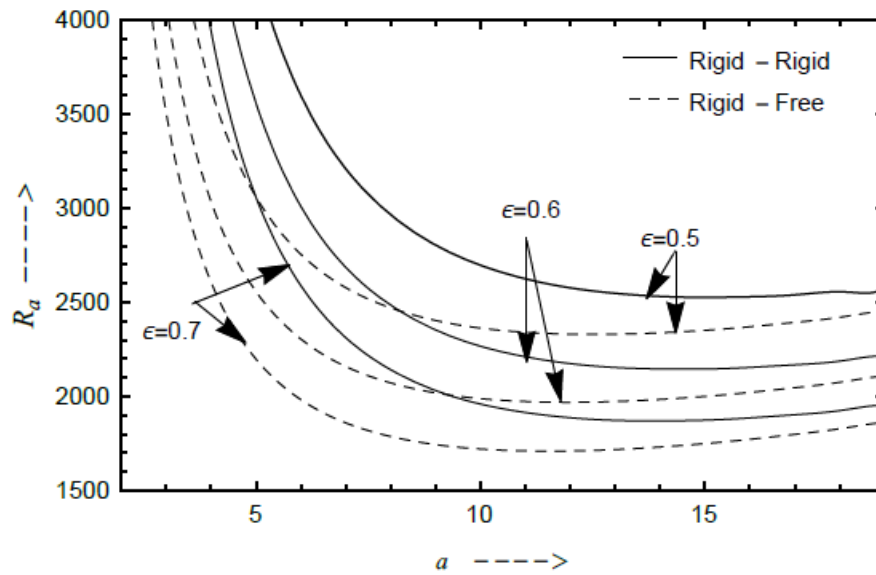


Figure 6. Influence of porosity on $R_a(stat)$ for $\epsilon=0.5, 0.6$ and 0.7 for two different boundaries

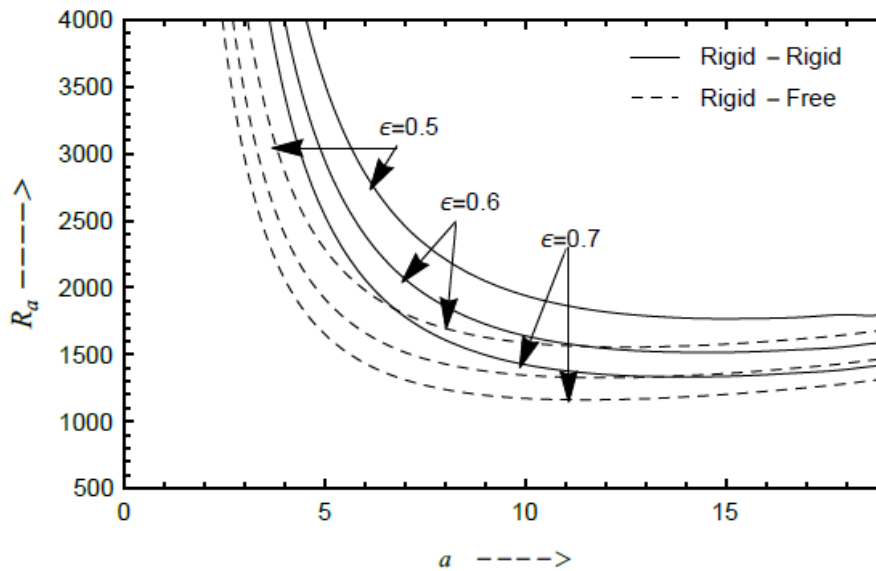


Figure 7. Influence of porosity on $R_a(osc)$ for $\epsilon=0.5, 0.6$ and 0.7 for two different boundaries

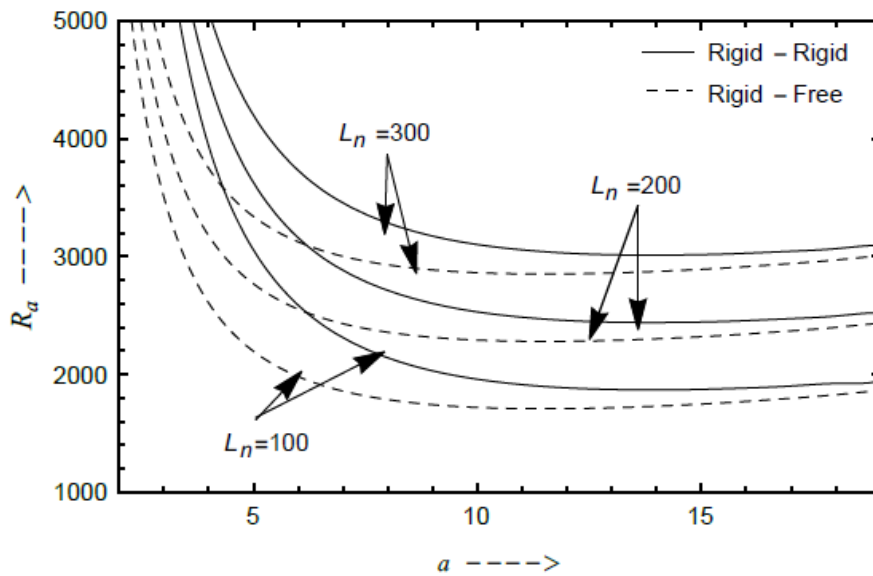


Figure 8. Influence of Lewis number on $R_a(stat)$ for $L_n=100, 200$ and 300 for three different boundaries

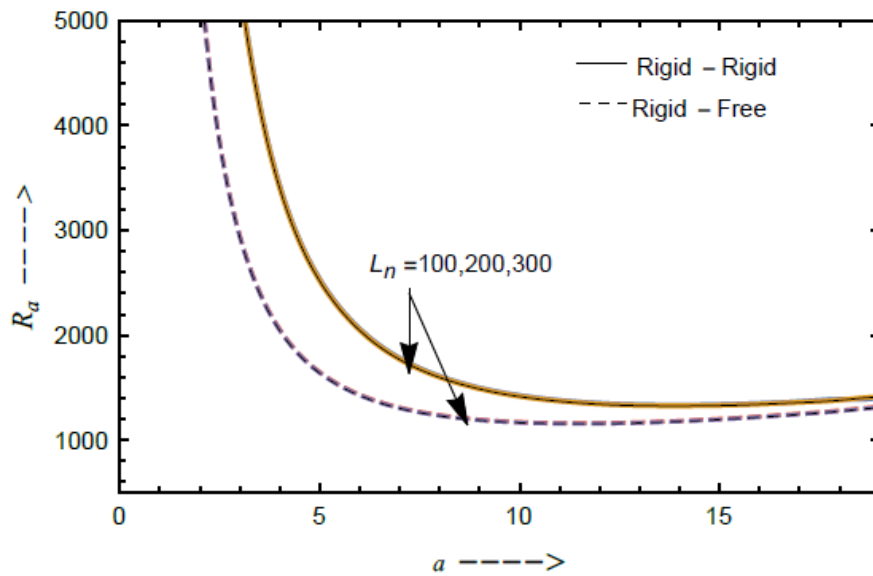


Figure 9. Influence of Lewis number on $R_a(osc)$ for $L_n=100, 200$ and 300 for three different boundaries

Figures 6-7 show the variation of Rayleigh number $R_a(stat)$ and $R_a(osc)$ for $\varepsilon=0.5, 0.6$ and 0.7 , respectively for rigid-rigid and rigid-free boundaries. As shown for alumina-water nanofluid, increase in porosity hastens the onset of oscillatory as well as non-oscillatory convection.

Figures 8-9 show the impact of Lewis number on the convection problem for $L_n=100, 200$ and 300 . It has been observed that with the rise in L_n , $R_a(stat)$ increases predominantly and $R_a(osc)$ does not show any significant change. Both rigid boundaries are more stable as compared to rigid-free boundaries.

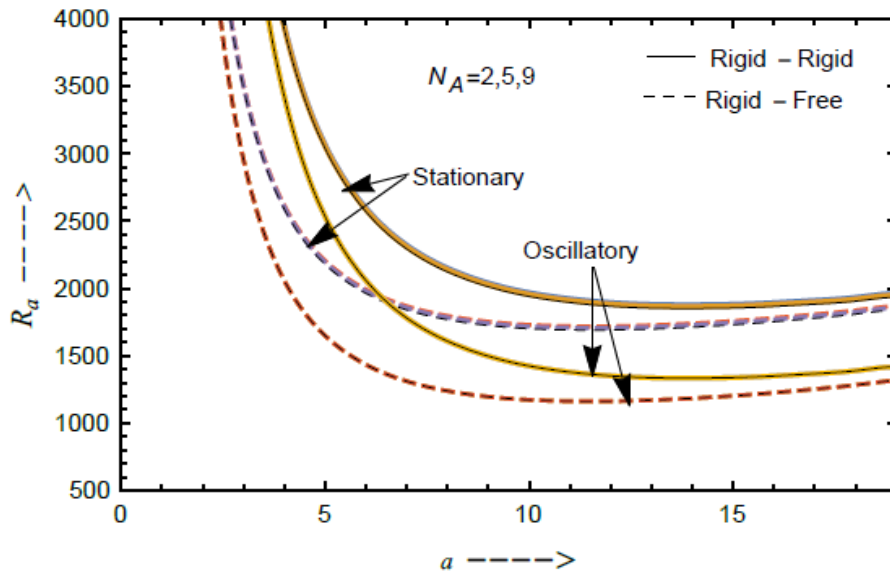


Figure 10. Influence of modified diffusivity ratio on $R_a(stat)$ and $R_a(osc)$ for $N_A = 2, 5$ and 9 for three different boundaries

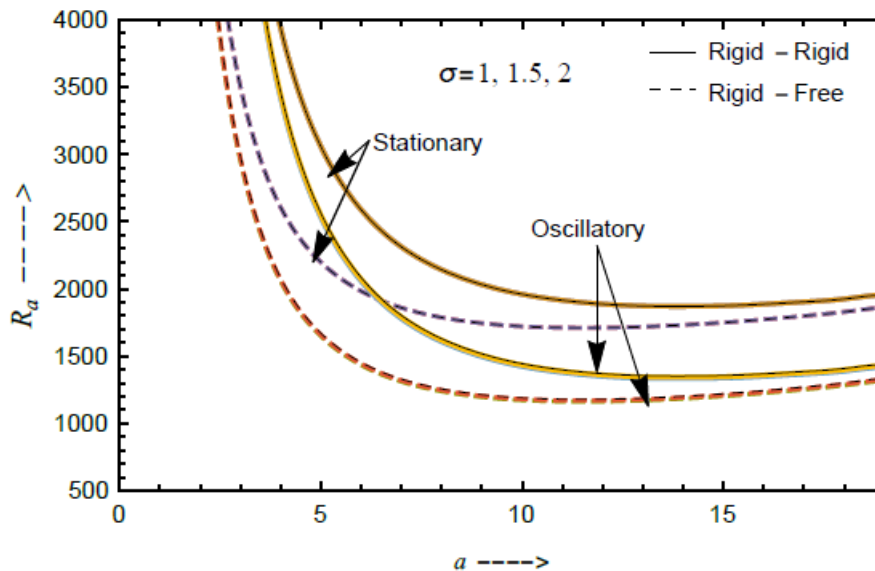


Figure 11. Influence of heat capacity ratio on $R_a(stat)$ and $R_a(osc)$ for $\sigma=1,1.5$ and 2 for three different boundaries

Figure 10 depicts the variation of $R_a(stat)$ and $R_a(osc)$ for $N_A=2,5$ and 9 for the two boundary conditions. In addition to the observation that the mode of instability is overstability, it is found that $R_a(stat)$ and $R_a(osc)$ are independent of the effect of diffusivity ratio. Figure 11 corresponds to $R_a(stat)$ and $R_a(osc)$ for $\sigma=1,1.5$ and 2. $R_a(stat)$ is independent of the heat capacity ratio and $R_a(osc)$ slightly rises with the rise in σ (not seen in graphs). This is due to the fact that Eqs. (37), (52) are (57) are independent of the heat capacity ratio. The convection sets in through oscillatory motions and $R_a(osc)$ for both rigid boundaries is much more than that for rigid-free boundaries.

8. Conclusions

The present article investigates Rayleigh-Bénard convection for nanofluids under the influence of magnetic field for more realistic boundary conditions: rigid-free and rigid-rigid. The solution of the eigen value problem is found in terms of Rayleigh number by implementing the technique of normal modes and weighted residual Galerkin approximation. It has been found that the mode of heat transfer is through oscillatory motions. It is expected as buoyancy forces are acting oppositely. The critical values of wave number and Rayleigh number are found for alumina-water nanofluid. It is observed that R_c shows a predominant fall with the increase in the ratio of pore space to total space for all the boundaries. As one moves from rigid-free boundaries to both rigid boundaries a_c shows an appreciable increase along with moderate increase in R_c . Both a_c and R_c exhibit a substantial increase as the Lorentz force is increased which shows that magnetic field strongly delays the onset of thermal convection. When magnetic field and nanoparticles are not present in the nanofluid layer, a_c and R_c for rigid-free boundaries are found to be 3.97 and 56.97, respectively, which lie below the critical wave number and critical Rayleigh number for both

rigid boundaries ($a_c=4.791$, $R_c=72.94$) for fixed value of porosity $\varepsilon=0.7$. The nanofluid layer system with both rigid boundaries is comparatively stable than rigid-free boundaries. To analyse the behavior of parameters like R_{cn} , Q , ε , L_n , N_A and σ computations are carried out using the software Mathematica to find $R_a(stat)$ and $R_a(osc)$. When the nanoparticle density decreases upward; the concentration Rayleigh number makes the stationary convection much more stable as compared to over stable motions. Lewis number is found to have dual character stabilizing for stationary convection and destabilizing for the oscillatory mode. It is also found that $R_a(stat)$ and $R_a(osc)$ are independent of the diffusivity ratio. As far as the effect of heat capacity ratio is concerned $R_a(stat)$ is independent of it whereas $R_a(osc)$ shows a slight rise with the rise in heat capacity ratio.

Appendix B1: Expression for $R_a(osc)$ for Rigid-rigid Boundaries

Separating the real and imaginary parts of Eq.(52) after putting $n = i\omega \neq 0$, we get an expression of $R_a(osc)$ for the rigid-rigid boundaries as

$$\begin{aligned}
 R_a(osc) = & \left[141120L_n Pr_1 Q\sigma + 17472L_n Pr_1 Qa^2\sigma + 270L_n Pr_2 R_{cn}a^2\sigma + 336L_n Pr_1 Qa^4\sigma \right. \\
 & + 27L_n Pr_2 R_{cn}a^4\sigma + 141120L_n Pr_1 \varepsilon\sigma + 33600Pr_2 \varepsilon\sigma + 20832L_n Pr_1 a^2\varepsilon\sigma + 9520Pr_2 a^2\varepsilon\sigma \\
 & - 270N_A Pr_2 R_{cn}a^2\varepsilon\sigma + 952L_n Pr_1 a^4\varepsilon\sigma + 896Pr_2 a^4\varepsilon\sigma - 27N_A Pr_2 R_{cn}a^4\varepsilon\sigma + 28L_n Pr_1 a^6\varepsilon\sigma \\
 & + 28Pr_2 a^6\varepsilon\sigma + 141120Pr_1 Q\sigma^2 + 17472Pr_1 Qa^2\sigma^2 + 252L_n Pr_1 R_{cn}a^2\sigma^2 + 336Pr_1 Qa^4\sigma^2 \\
 & + 27L_n Pr_1 R_{cn}a^4\sigma^2 + 141120Pr_1 \varepsilon\sigma^2 + 20832Pr_1 a^2\varepsilon\sigma^2 + 952Pr_1 a^4\varepsilon\sigma^2 + 28Pr_1 a^6\varepsilon\sigma^2 \\
 & \left. - 336L_n Pr_2 \varepsilon\omega^2 - 28L_n Pr_2 a^2\varepsilon\omega^2 \right] \left[(9a^2\varepsilon\sigma)(28L_n Pr_1 + 30Pr_2 + 3L_n Pr_1 a^2 + 3Pr_2 a^2) \right]^{-1},
 \end{aligned}
 \tag{B.1.1}$$

where $\omega^2 = \frac{-X_2 + \sqrt{X_2^2 - 4X_1X_3}}{2X_1}$, which is obtained by eliminating $R_a(osc)$ between real and imaginary parts of the eigen value Eq. (52) and X_1, X_2, X_3 are the coefficients of the biquadratic equation $X_1\omega^4 + X_2\omega^2 + X_3 = 0$.

Appendix B2: Expression for $R_a(osc)$ for Rigid-Free Boundaries

In this case the eigen value Eq. (57) gives the expression for $R_a(osc)$ by separating real and imaginary parts as

$$\begin{aligned}
 R_a(\text{osc}) = & \left[1270080L_n Pr_1 Q\sigma + 187488L_n Pr_1 Qa^2\sigma + 5070L_n Pr_2 R_{cn} a^2\sigma + 6048L_n Pr_1 Qa^4\sigma \right. \\
 & + 507L_n Pr_2 R_{cn} a^4\sigma + 1270080L_n Pr_1 \varepsilon\sigma + 604800Pr_2 \varepsilon\sigma + 247968L_n Pr_1 a^2\varepsilon\sigma + \\
 & 174160Pr_2 a^2\varepsilon\sigma - 5070N_A Pr_2 R_{cn} a^2\varepsilon\sigma + 17416L_n Pr_1 a^4\varepsilon\sigma + 16688Pr_2 a^4\varepsilon\sigma \\
 & - 507N_A Pr_2 R_{cn} a^4\varepsilon\sigma + 532L_n Pr_1 a^6\varepsilon\sigma + 532Pr_2 a^6\varepsilon\sigma + 1270080Pr_1 Q\sigma^2 \\
 & + 187488Pr_1 Qa^2\sigma^2 + 4914L_n Pr_1 R_{cn} a^2\sigma^2 + 6048Pr_1 Qa^4\sigma^2 + 507L_n Pr_1 R_{cn} a^4\sigma^2 \\
 & + 1270080Pr_1 \varepsilon\sigma^2 + 247968Pr_1 a^2\varepsilon\sigma^2 + 17416Pr_1 a^4\varepsilon\sigma^2 + 532Pr_1 a^6\varepsilon\sigma^2 \\
 & \left. - 6048L_n Pr_2 \varepsilon\omega^2 - 532L_n Pr_2 a^2\varepsilon\omega^2 \right] \left[(36L_n a^2\varepsilon\sigma)(126Pr_1 + 130Pr_2 + 13Pr_1 a^2 + 13Pr_2 a^2) \right]^{-1},
 \end{aligned}
 \tag{B.1.2}$$

where $\omega^2 = \frac{-X_2 + \sqrt{X_2^2 - 4X_1X_3}}{2X_1}$, is obtained in the same manner as for rigid-rigid boundaries and X_1, X_2, X_3 are the coefficients of the biquadratic equation $X_1\omega^4 + X_2\omega^2 + X_3 = 0$.

Conflict of Interest

The authors confirm that there is no conflict of interest to declare for this publication.

Acknowledgement

The research work presented in this chapter has been supported by grants to second author from CSIR, New Delhi-110012, India via Project [Ref. No: 25(0247)/15/EMR-II].

References

- Bhadauria, B. S., & Agarwal, S. (2011). Natural convection in a nanofluid saturated rotating porous layer: A Nonlinear study. *Transport in Porous Media*, 87(2), 585–602.
- Buongiorno, J. (2006). Convective transport in nanofluids. *ASME Journal of Heat Transfer*, 128(3), 240–250.
- Buongiorno, J. and Hu, W. (2005). Nanofluid coolants for advanced nuclear power plants. *Paper No. 5705, Proceedings of ICAPP'05, Seoul*.
- Chandrasekhar, S. (1981). *Hydrodynamic and hydromagnetic stability*. New York: Dover Publications.
- Choi, S. (1995). Enhancing thermal conductivity of fluids with nanoparticles: *Development and Applications of Non-Newtonian flows*. ASME FED- 231/MD-vol. 66, 99–105.
- Das, S. K., Putra, N., Thiesen, P., & Roetzel, W. (2003). Temperature dependence of thermal conductivity enhancement for nanofluids. *ASME Journal of Heat Transfer*, 125(4), 567–574.
- Gupta, U., & Ahuja, J. (2014). Hall Effect on thermal convection of a nanofluid layer saturating a porous medium. *International Journal of Technology*, 4(1), 214-219.
- Gupta, U., Ahuja, J., & Wanchoo, R. K. (2013). Magneto convection in a nanofluid layer. *International Journal of Heat and Mass Transfer*, 64, 1163–1171.

- Heris, S. Z., Salehi, H., & Noie, S. H. (2012). The effect of magnetic field and nanofluid on thermal performance of two phase closed thermosyphon. *International Journal of Physical Sciences*, 7(4), 534–543.
- Kim, J., Kang, Y. T., & Choi, C. K. (2004). Analysis of convective instability and heat transfer characteristics of nanofluids. *Physics of Fluids*, 16(7), 2395–2401.
- Kleinstreuer, C., Li, J., & Koo, J. (2008). Microfluidics of nano-drug delivery. *International Journal of Heat and Mass Transfer*, 51(23-24), 5590–5597.
- Masuda, H., Ebata, A., Teramae, K., & Hishinuma, N. (1993). Alteration of thermal conductivity and viscosity of liquid by dispersing ultra fine particles. *Netsu Bussei*, 7(4), 227–233.
- Nield, D. A., & Kuznetsov, A. V. (2009). Thermal instability in a porous medium layer saturated by a nanofluid. *International Journal of Heat and Mass Transfer*, 52(25-26), 5796–5801.
- Nield, D. A., & Kuznetsov, A. V. (2010). The onset of convection in a horizontal nanofluid layer of finite depth. *European Journal of Mechanics- B/Fluids*, 29(3), 217–223.
- Tzou, D.Y. (2008). Instability of nanofluids in natural convection. *ASME Journal of Heat Transfer*, 130(7), 372–401.
- Yadav, D., Agrawal, G. S., Bhargava, R. (2011). Thermal instability of rotating nanofluid layer. *International Journal of Engineering Science*, 49(11), 1171–1184.